ACS APPLIED MATERIALS & INTERFACES

Research Article

www.acsami.org

Influence of Pyrene Grafting on PMMA Nanosecond Laser Ablation at 248 nm

Emeric Biver,*[,†] Marco Berta,[‡] Anthony D'Aléo,[§] Trang Phan,[‡] Sébastien Maria,[‡] Frédéric Fages,[§] Didier Gigmes,[‡] Marc Sentis,[†] and Philippe Delaporte[†]

[†]LP3 UMR 7341 and [§]CINaM UMR 7325, Aix Marseille Université, CNRS, 13288, Marseille, France

[‡]ICR UMR 7273, CNRS, Aix Marseille Université, 13397 Marseille, France

Supporting Information

ABSTRACT: In this work, we investigate the effects of KrF nanosecond laser ablation on poly(methyl methacrylate) (PMMA) in combination with pyrene. Three materials containing PMMA were studied: (1) one doped with pure pyrene, (2) one doped with methyl 3-(1-pyrenyl)propanoate (so called alkylpyrene derivative thereafter), and (3) one grafted with pyrene. This last new material was developed by covalently bonding pyrene molecules to PMMA side-chains. A comparative study was undertaken to determine and compare the respective properties of the PMMA dye containing pyrene during nanosecond laser ablation at 248 nm. Cavities were etched for each material with up to 20 pulses for fluences between 0.03 and 1.7 J/cm^2 in samples containing 1, 2, and 4 mol % chromophore. The threshold fluences and the effective absorption coefficients were obtained. It was observed that effective absorption coefficients increased and threshold fluences decreased with the chromophore percentages in each kind of sample. Ablation parameters were not significantly modified when the dopant was changed from pyrene to the alkylpyrene derivative. On the other hand, when pyrene molecules were grafted on the polymer, the threshold fluences decreased, whereas the effective absorption coefficients became similar at fluences above 0.6 J/cm^2.

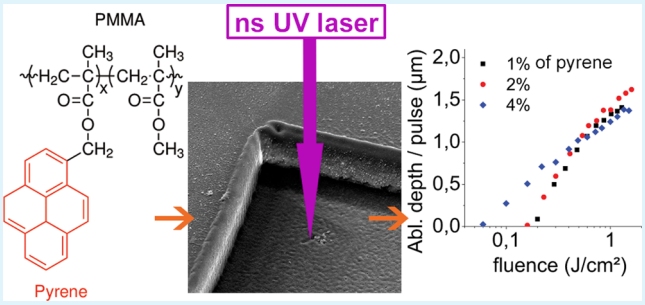

KEYWORDS: *laser ablation, PMMA, pyrene, functionalization, aggregation, chromophore, effective absorption, threshold fluence*

INTRODUCTION

Microelectronics in organic substrates is a promising field of application for laser processes as the latter can add versatility and flexibility. For example, to fabricate embedded arrays of interconnected microelectronics components inside plastic foils, lasers can efficiently etch cavities, place microchips inside the cavities and connect them.[1] The quality of laser ablation of polymers depends highly on the polymer itself, in addition to the laser wavelength or pulse width.[2] It is therefore useful to consider tuning the materials' properties to improve their ability to be efficiently etched by laser irradiation.

Since its beginnings 30 years ago, excimer laser ablation of polymers has been extensively studied.[3−5] One chemical way to enhance the ablation consists in designing polymers that incorporate a photosensitive group into their main chains. Therefore, upon laser irradiation, the polymer main chain is fragmented and decomposed into volatile species.[6] Further, such polymers have been proven to present both a lower threshold fluence and a higher ablation depth per pulse than standard commercial polymers used for microelectronics components.[2] Another way to improve laser ablation of polymers, less efficient but easier and cheaper, is to disperse the photosensitive molecules into the polymer matrix by simple mixing, i.e., doping. Poly-aromatic compounds are especially well suited as dopants.[7,8] When irradiated, the dopants efficiently absorb the laser energy and are thermally activated. Vibrational processes transmit the energy to the surrounding polymer matrix, enhancing thermal ablation.[9,10] When sufficient amounts of dopant are well-dispersed in the polymer matrix, clean ablation cavities are obtained because the energy is deposited homogeneously in the material.[11]

In this work, we investigate the KrF excimer laser ablation of PMMA using pyrene as a chromophore (Scheme 1). PMMA is a weakly absorbing polymer exhibiting high incubation behavior.[12] The effect of pyrene as a dopant upon UV laser ablation of PMMA was investigated by Fujiwara and colleagues

Scheme 1. Chemical Formula of (a) PMMA and (b) Pyrene

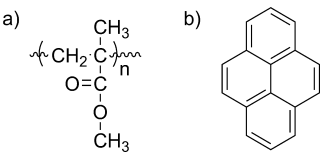

Received: November 27, 2012
Accepted: December 16, 2013
Published: December 16, 2013

in the 1990s.[13] In that work, the authors showed that pyrene is not decomposed upon irradiation, in spite of the many photons it successively absorbs during the pulse. Ablation is thus dominated by thermal processes and governed by the absorbing and thermal conductivity properties of the doped polymer. Pyrene, like other polycyclic aromatic hydrocarbons, tends to aggregate to minimize its energy[14] which can be a limiting factor for laser ablation because it can decrease the homogeneity of the samples and negatively impact the quality of ablation. To limit this aggregation phenomenon, two different strategies were used: (1) increase of the solubility of the pyrene unit to avoid the fast aggregation process (addition of an alkyl group terminated by an ester function, Scheme 2a) and (2) dispersion of the pyrene moieties by incorporating the dye into PMMA block copolymer. In the latter case, a new material was synthesized by attaching a hydroxymethyl derivative of pyrene to the methacrylate monomer (Scheme 2b) and then copolymerizing these modified monomers with methyl methacrylate (MMA) (Scheme 2c). In the resulting material, the pyrene molecules were not inserted into the main chain but rather grafted on the side chains to enhance dispersion.

Scheme 2. Chemical Formula of (a) Methyl 3-(1-Pyrenyl)propanoate (the alkylpyrene derivative used in this study), (b) Pyren-1-ylmethyl Methacrylate Monomer, and (c) Pyrene-Grafted PMMA

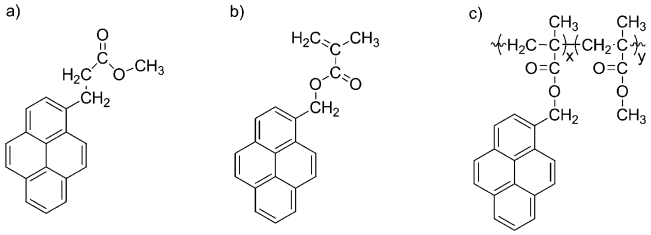

EXPERIMENTAL SECTION

Materials. Methyl methacrylate (MMA, 99%), pyrene (98%), 1-pyrenemethanol (98%), methacryloyl chloride (97%), and benzoyl peroxide (BPO, 75%) were all purchased from Sigma-Aldrich and used without further purification. Methyl 3-(1-pyrenyl)propanoate (Scheme 2a), referred to hereafter as alkylpyrene derivative,[15] was prepared according to the synthesis procedure described elsewhere.[16]

Synthesis of 1-Pyrenemethyl Methacrylate (PyMMA) (Scheme 2b). Pyrene methacrylate monomer was synthesized following the procedure described by Jiang and colleagues.[17] Typically, 1-pyrenemethanol (5 g; 0.022 mol) was added to a solution of triethylamine (9.0 mL; 0.065 mol) in 250 mL of dried tetrahydrofurane (THF). Methacryloyl chloride (6.3 mL; 0.065 mol) was added dropwise under stirring at 0 °C. The reaction was conducted at room temperature overnight. The reaction medium was filtered, THF was evaporated, and the solid residue was dissolved in dichloromethane (300 mL). This solution was washed with 1.0 M HCl solution, and then with an aqueous solution of sodium hydrogen carbonate, and finally with water. After drying over magnesium sulfate ($MgSO_4$), the organic solution was filtered, and the solvent was evaporated under reduced pressure. A yellow solid was collected, dissolved in 5 mL of THF, and precipitated by the addition of 10 mL of methanol. After one night at −20 °C, the product was collected by filtration and dried under a vacuum at room temperature.

Synthesis of PMMA. Polymer was synthesized by conventional radical polymerization in bulk at 80°C in the presence of 0.25 wt % BPO. When the mixture viscosity increased significantly, MMA polymerization was stopped by quenching the reactor in a cold water bath. The mixture was then dissolved with THF and PMMA was recovered by precipitation in ethanol and dried at room temperature.

Synthesis of Poly(MMA-*co*-PyMMA) (Scheme 2c). In a typical experiment, 0.5 g of PyMMA (1.7 mmol), 0.025 g of BPO (0.10 mmol), 10 mL of MMA (95 mmol) and 3.5 mL of toluene were added to a glass reactor. The mixture was purged with argon for 20 min to remove oxygen and then heated at 80°C with stirring overnight. After cooling to 25 °C, 10 mL of toluene was added, and the polymer was recovered by precipitation in cold ethanol and dried.

Polymer Film Preparation for Laser Ablation. Dried polymers (PMMA or P(MMA-co-PyMMA)) were dissolved in THF at a concentration of 75 g/L. Polymer films with a thickness of 100−200 μm were obtained by casting this solution into aluminum cups upon solvent evaporation. For samples prepared by the doping method, the desired amount of pyrene or alkylpyrene derivative was added to PMMA solution before casting of the polymer solution into the Al cups.

Laser Ablation. The laser used for this study was a Lambda-Physik LPX200 excimer laser (pulse duration, 30 ns; wavelength, 248 nm). A mask was used to select a small and homogeneous part of the laser beam. The angle of a coated quartz plate placed in the beam trajectory was changed to control the transmitted energy deposited on the sample. The beam was then focused by a quartz lens with a focal length of 300 mm. The sample consisted of thin polymer films fixed on a holder and placed perpendicular to the beam. It was positioned to image the mask, through the lens, on the surface of the film, thus yielding square homogeneous energy deposition. Edge steepness and plateau uniformity (ISO 13694)[18] were 0.911 and 0.024, respectively, as checked by a SP620U Spiricon CCD camera. Cavities were etched in air (ambient temperature, average humidity of ∼55%) with a controlled number of laser shots and a pulse repetition rate of 2 Hz to avoid cumulative heating. The spots always had the same dimension, namely 500 μm by 500 μm. An aspiration system was used to avoid redeposition of the ablation products. The energy was measured with a Gentec Maestro joulemeter

Characterization. Several techniques were used in order to characterize the samples both before and after laser ablation. Nuclear magnetic resonance (NMR) spectroscopy was the technique used to check the purity of the final grafted PMMA. NMR spectra were recorded at 400 MHz in $CDCl_3$ solutions with a Bruker Avance 400 spectrometer. The number average molecular weight, M_n, and weight average molecular weight, M_w, were determined via size-exclusion chromatography (SEC) analysis. They were realized on an EcoSEC system (Tosoh) composed of a reference pump, a sample pump, a pressure generator as "reference column," a sample column, a UV detector at 254 nm and a dual-flow refractive index detector, all thermostated at 40°C. The mobile phase was pure stabilized THF previously filtered on a 0.2 μm Alltech PTFE membrane. The flow-rate of the reference part was fixed at 0.15 mL/min and the flow-rate of the sample part is fixed at 0.3 mL/min. The sample part stationary phase was a set of PL-Resipore columns (Guard column measuring 40 × 4.6 mm^2 and two Linear M columns measuring 250 × 4.6 mm^2, Agilent). The system was calibrated by using PMMA standards with molar masses between 1.85 and 520 kg/mol. PMMA standards and samples were solubilized in THF containing 0.25 wt % toluene (as flow marker), at a concentration of 0.25 wt % for 24 h. They were then filtered on a PTFE syringe filter with dimensions 0.2 μm × 25 mm. The injection volume was 20 μL per sample.

Fluorescence spectroscopy measurements were performed directly on the solvent-cast films with a Horiba-Jobin Yvon Fluorolog-3 spectrofluorimeter, equipped with three-slit double-grating excitation and spectrograph emission monochromator with dispersions of 2.1 nm/mm (1200 grooves/mm). Steady-state luminescence was excited by unpolarized light from a 450W xenon CW lamp at 320 nm and detected in a front face configuration on PMMA films by a red-sensitive Hamamatsu R928 photomultiplier tube.

For the acquisition of UV−visible electronic absorption spectra, thin films were prepared on quartz plates by spin-coating a polymer solution in THF at a concentration of 7.5 g/L. The spin coater was turned on at 2000 rpm for 60 s with a speed ramp of 500 rpm/s. UV−

visible electronic absorption spectra were recorded with a Varian Cary 50 UV spectrophotometer.

Doped and grafted PMMA films were also observed under a Zeiss LSM 700 confocal microscope to evaluate the homogeneity of pyrene distribution and its possible aggregation.

Scanning electron microscopy was used to check the overall aspect of the cavities with a JEOL JSM-6390 scanning electron microscope (acceleration voltage of 10 kV), from samples on which ~20 nm of gold was evaporated. Depth measurements of the ablated craters were performed with a Leica DCM 3D confocal microscope.

RESULTS AND DISCUSSION

Chemical Characterization of Pyrene-Grafted PMMA. During the synthesis of the pyrene-grafted PMMA, the grafted monomers were found to be less reactive than the MMA monomers. This can be partly attributed to the pre-associated pyrene groups in stacked structures and the steric hindered structure of PyMMA. SEC analyses were used to characterize the materials. Chromatograms of pure PMMA and pyrene-grafted PMMA are shown in Figure 1. The determined number

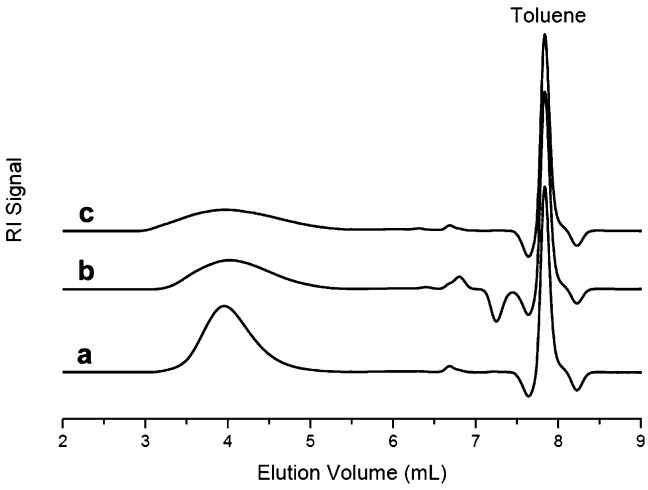

Figure 1. Overlaid SEC chromatograms of (a) pure PMMA, (b) pyrene-grafted PMMA 2%, and (c) pyrene-grafted PMMA 4%.

average molecular weights (M_n) and polydispersity index ($Đ$) are given in Table 1. The pyrene-grafted PMMA is more

Table 1. Molar Masses and Polydispersity Index Determined by SEC

samples	M_n (g mol^{-1})	$Đ$
pure PMMA	216 000	2.07
pyrene-grafted PMMA 5%	142 000	3.07
pyrene-grafted PMMA 8%	128 000	4.58

polydispersed than the pure PMMA because of its different chemical structure. Indeed, $Đ$ increases with the content of pyrene. Molar masses are quite similar in all samples. No UV signal was measured for the pure PMMA sample, whereas UV and Refractive Index signals were well overlaid for the pyrene-grafted PMMA sample (see the Supporting Information). This is due to the presence of the pyrene groups that absorb at 254 nm, and proves that pyrene is well-grafted on PMMA. Moreover, NMR spectra of grafted PMMA show that no dispersed monomer is present (see the Supporting Information).

Throughout the article, three concentrations are mentioned for the proportion of pyrene in the samples: 1, 2, and 4%. These correspond to molar percentages of the chromophore molecule. Table 2 is a summary of the measured molar

Table 2. Real Chromophore Molar Percentages for the Samples Studied and the Error (in mol %) for the Pyrene-Grafted PMMA Samples

	theoretical pyrene mol %		
sample	1	2	4
pyrene-doped PMMA	0.98%	1.94%	3.81%
alkylpyrene derivative-doped PMMA	0.97%	1.90%	3.78%
pyrene-grafted PMMA	0.89%	1.59%	3.64%
error on the measurement (for pyrene-grafted PMMA)	0.12%	0.13%	0.19%

concentrations of pyrene or pyrene derivatives for each kind of sample. The real values differ slightly from the theoretical ones, but the latter are used for the sake of simplicity of notation. The errors in the doped samples mol % are estimated as less than 0.2 mol %. The percentage of grafted pyrene could be estimated by the intensity of absorbance peaks on UV-visible electronic absorption spectra, after calibration with doped films where the amount of pyrene was carefully adjusted, and measurement of film thickness. The errors on percentages obtained this way are higher than those for the other two kinds of samples and are included in Table 2. They come from the standard errors of the fitting coefficients for the calibration with doped samples electronic absorption spectra.

UV−Visible Electronic Absorption Spectroscopy. UV−visible electronic absorption spectra were measured from thin films spin-coated on quartz plates because this technique requires much thinner films than those obtained by solvent-casting. The PMMA molar absorption coefficient at 248 nm is very low compared with pyrene. Therefore, when PMMA and pyrene are mixed, it is mainly pyrene that absorbs light at this wavelength. The linear absorption coefficient α_0 increases with the percentage of pyrene added to the polymer.

Figure 2 shows linear absorption spectra, obtained from UV-Visible electronic absorption spectra, for pure PMMA and PMMA doped with pyrene, the alkylpyrene derivative and grafted with pyrene. Functionalization of pyrene at the 1-position for the alkylpyrene derivative and the grafted pyrene

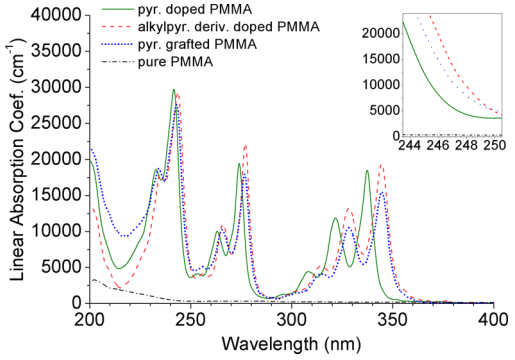

Figure 2. Linear absorption coefficient α_0 (cm^{-1}) from UV−visible electronic absorption spectra for pure PMMA, PMMA doped with pyrene, PMMA doped with the alkylpyrene derivative, and PMAA grafted with pyrene. The concentration of pyrene chromophore was 2 mol % (inset: zoom around 248 nm).

dx.doi.org/10.1021/am404376e | ACS Appl. Mater. Interfaces 2014, 6, 41−48

induces a red shift of the spectrum for the three absorption bands[19] because of a break in the molecule symmetry.[20] The β-band (~215−250 nm) of the grafted pyrene and alkylpyrene derivative samples is red-shifted by 1 and 2 nm, respectively, compared with that of the pyrene-doped samples. In Figure 2, we observe an increase of the absorption at 248 nm for functionalized pyrene samples (inset). Measured values of α_0 for PMMA doped with pyrene, the alkylpyrene derivative and grafted with pyrene are 4215, 9695 and 7900 cm^{-1}, respectively. These values have an error of ±15% which derives from thickness measurements and diffusion corrections. In consequence, those values have to be treated with caution. There does, however, seem to be an increase in α_0 upon pyrene functionalization.

Fluorescence Spectroscopy. Fluorescence spectroscopy was used to qualitatively monitor the aggregation of pyrene molecules. Steady-state emission spectra were recorded on films containing various percentages of chromophore for the three kinds of samples under study. Figure 3 shows steady-state emission spectra measured on films containing respectively 1, 2, and 4% of chromophore for the three kinds of samples under study (excitation wavelength: 320 or 330 nm). Intensities are normalized to the first peak and each curve is an average of several spectra taken at different locations on the samples, to mitigate the effect of possible inhomogeneities.

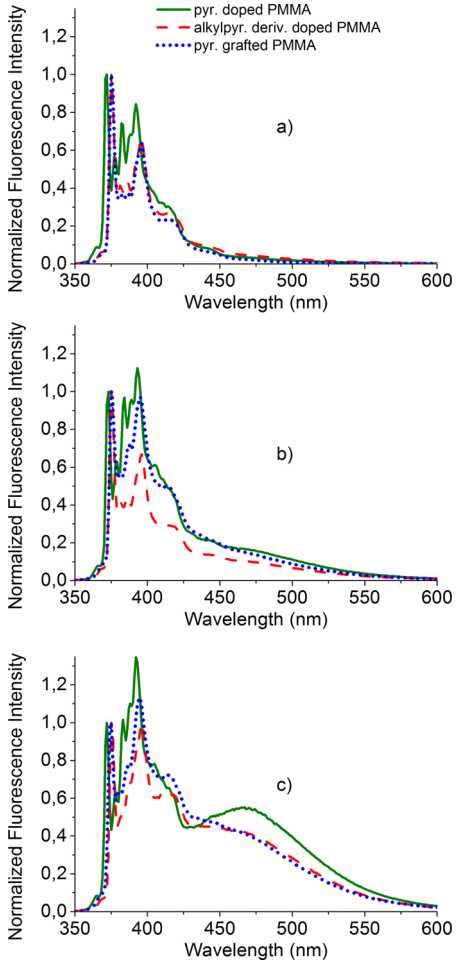

Figure 3. Fluorescence spectra of PMMA doped with pyrene, doped with alkylpyrene derivative, and grafted with pyrene, with 3 chromophore concentrations: (a) 1, (b) 2, and (c) 4 mol% (excitation wavelength: 320 or 330 nm).

At low pyrene percentages (Figure 3a), we observe the characteristic structured fluorescence emission profile of the isolated pyrene monomer between 360 and 430 nm. The effects of pyrene functionalization are a red shift and a modification of the relative heights of the emission bands. At higher pyrene percentages (Figure 3b, c), a large structureless emission band centered on 465 nm for non-functionalized pyrene appears, which is attributed to the excimer-like transition of pre-associated pyrene molecules.[14,21] This band is blue-shifted for functionalized pyrene. For the three kinds of samples under study, the aggregated emission band increases with the percentage of pyrene, revealing that an increasing proportion of pyrene is stacked. When the pyrene concentration is sufficiently high (above 6%), some spectra no longer contain fluorescence emission of free pyrene units (spectra not shown).

One might expect an improvement of the solubility of the functionalized pyrene samples compared with the non-functionalized ones,[22] as well as a change in the way pyrene is stacked. Unfortunately, the fluorescence data do not allow quantitative comparison of pyrene aggregation between the three types of samples since the pyrene monomer to excimer quantum yield ratios are not known and may change with functionalization. Nevertheless, aggregation was observed in all samples at sufficient chromophore concentration, indicating that pyrene molecules may still get close enough to preassociate, even when grafted to the main polymer backbone.

The alkylpyrene derivative and the grafted pyrene are functionalized in a similar way (an alkyl bridge in position 1, see Scheme 2). It therefore seems reasonable, even if the quantum yields of pre-associated pyrenes are not known, to postulate that they should be very close for both functionalized samples. Consequently we suggest that the aggregation is similar for the two functionalized pyrene samples because their spectra are similar at each concentration (Figure 3).

Laser Ablation: Aspect and Ablation Depths. Selected SEM micrographs of cavities made on the three kinds of samples with three different percentages of pyrene are shown in Figure 4. The cavities were made by 20 pulses at a fluence of 1.1 J/cm^2. Ablation depths per pulse for cavities etched at 0.35 and 1.1 J/cm^2 are reported in Table 3.

KrF laser ablation of undoped PMMA is explosive and produces bubbles, projections and a very high roughness. As mentioned previously, pyrene is used as a chromophore because it enhances the absorption of the laser pulse and induces thermal ablation.[13] The micrographs of Figure 4 are organized so that the first line (Figure 4a−c) corresponds to pyrene-doped samples, the second line (Figure 4d−f) to the alkylpyrene derivative-doped samples and the third line (Figure 4g−i) to pyrene-grafted samples. The columns from left to right correspond to an increasing chromophore proportion, respectively 1% (Figure 4a, d, g), 2% (Figure 4b, e, h) and 4% (Figure 4c, f, i). Comparing the first column with the last column, we observe that the ablation quality increases with pyrene proportion. The edges, as well as the bottoms of the cavities, keep their melted aspect, evidence of thermal ablation, but become smoother; the number of projections around the cavity decreases; the number of melted filaments seen around the edges decreases in the case of pyrene (compare 4a with 4c) and completely disappear when pyrene is functionalized (compare 4d and 4g with 4f and 4i). As the chromophore concentration increases, the energy is deposited in a thinner

dx.doi.org/10.1021/am404376e | ACS Appl. Mater. Interfaces 2014, 6, 41−48

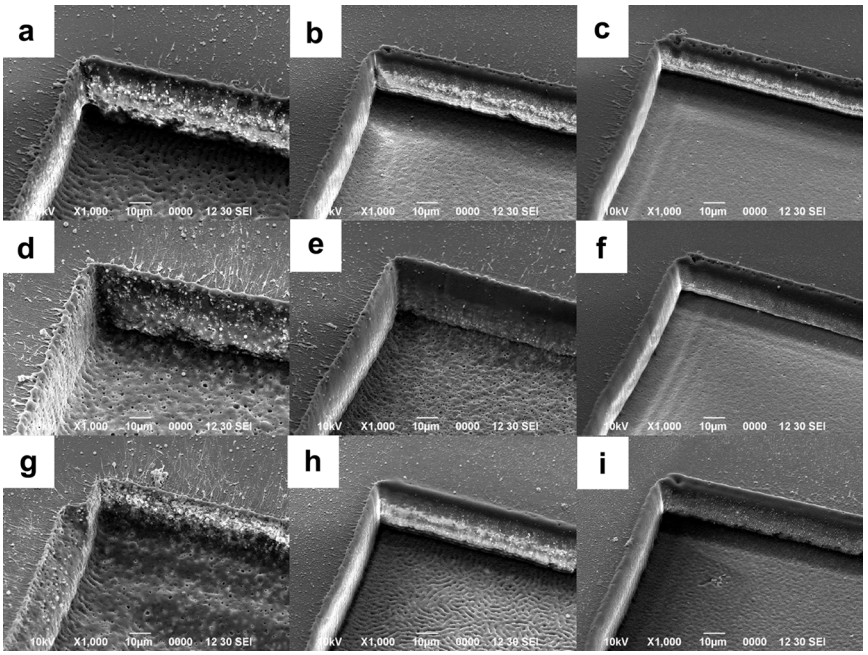

Figure 4. SEM micrographs of cavities done with 20 laser pulses at 1.1 J/cm^2; (a–c) pyrene-doped PMMA with 1, 2, and 4%, respectively; (d–f) the alkylpyrene derivative-doped PMMA with 1, 2, and 4%, respectively; (g–i) pyrene-grafted PMMA with 1, 2, and 4%, respectively.

Table 3. Measured Ablation Depths Per Laser Pulse in μm for Three Percentages of Pyrene and for Two Fluences

	fluence: 0.35 J/cm^2			fluence: 1.1 J/cm^2		
	mol % pyrene					
	1	2	4	1	2	4
pyrene-doped PMMA		0.6	0.6	1.8	1.4	1
alkylpyrene derivative-doped PMMA		0.6	0.6	1.7	1.4	1
pyrene-grafted PMMA	0.6	0.7	0.8	1.4	1.4	1.3

layer in the material. This increases the thermal gradients and decreases the proportion of material which is molten but not ablated. It results in cleaner ablation[10] but less deep cavities, as can be seen in Table 3. Interestingly, this effect is less pronounced for grafted samples. A slight patterning with a characteristic length scale can also be observed on the bottom of the cavity with 2% grafted pyrene. These spinodal motives may originate from the interaction between pre-associated pyrene molecules.

For the same chromophore concentration (for the micrographs of a given column in Figure 4), ablation quality is independent of the way in which pyrene is dispersed into the PMMA. Also, the comparison of the ablation depths per pulse for two fluences in Table 3 shows that the mere functionalization of the dopant does not seem to affect the crater depths, but the grafting on the polymer does. This is particularly evident if we compare the data for 1 and 4% of pyrene in Table 3. At the lower fluence of 0.35 J/cm^2, the cavities are less clean and the differences in ablation depth per pulse between materials are less significant (Table 3). When the profile was too irregular, no reliable depth measurement could be taken for the materials doped with 1% of chromophore. At this fluence, the pyrene-grafted PMMA gave the best response to laser ablation because measurable cavities were etched even with a low percentage of pyrene.

Effective Absorption Coefficients and Threshold Fluences. The threshold fluence and the effective absorption coefficient are two parameters that characterize laser ablation and can help to explain the previous observations. When the ablation depth per pulse varies linearly with the logarithm of the fluence, these parameters are defined according to the following formula

$$h(F) = \frac{1}{\alpha_{\text{eff}}} \ln\left(\frac{F}{F_{\text{th}}}\right) \quad (1)$$

where h, α_{eff}, F, and F_{th} are the ablation depth per pulse, the effective absorption coefficient, the fluence, and the threshold fluence, respectively.[4,9] The ablation threshold fluence describes the fluence above which ablation starts. Because undoped PMMA is a very transparent polymer, it has a strong incubation behavior. For a fluence close to the ablation threshold, the ablation may start only after several pulses that create absorbing centers and increase the linear absorption. Figure 5 shows ablation depths measured on cavities made in PMMA doped with 1% of pyrene after several pulses and for several fluences.

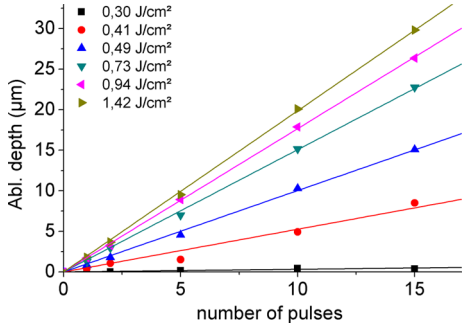

Figure 5. Ablation depths (in μm) according to the number of laser pulses for cavities etched in a 1% pyrene-doped PMMA sample at several fluences (lines are linear regressions).

dx.doi.org/10.1021/am404376e | ACS Appl. Mater. Interfaces 2014, 6, 41–48

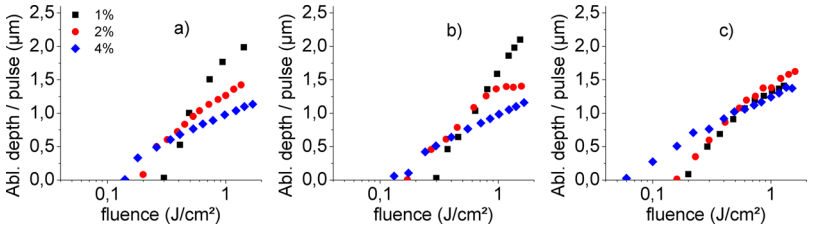

Figure 6. Ablation depth per pulse h (μm/pulse) according to the fluence for PMMA (a) doped with pyrene, (b) doped with the alkylpyrene derivative, and (c) grafted with pyrene, with 1, 2, and 4% chromophore.

Table 4. Effective Absorption Coefficients α_{eff} and Ablation Threshold Fluences F_{th} for the Studied Samples, As Extracted from the Graphs in Figure 6[a]

	α_{eff} (cm^{-1})			F_{th} (mJ/cm^2)		
	mol % pyrene					
sample	1	2	4	1	2	4
pyrene-doped PMMA	6400 (± 17%)	15 600 (± 15%)	27 500 (± 11%)	280 (± 7%)	160 (± 14%)	105 (± 25%)
alkylpyrene derivative-doped PMMA	8100 (± 3%)	13 600 (± 5%)	26 300 (± 5%)	276 (± 6%)	165 (± 2%)	105 (± 19%)
pyrene-grafted PMMA at F < 0.6 J/cm^2	12 300 (± 13%)	11 800 (± 8%)	21 200 (± 6%)	166 (± 12%)	152 (± 4%)	55 (± 4%)
pyrene-grafted PMMA at$F$ > 0.6 J/cm^2	23 300 (± 10%)	22 700 (± 12%)	28 600 (± 5%)			

[a]The relative errors correspond to standard deviations for several matching fits.

Similar graphs have been obtained for all materials and for all chromophore concentrations. Ablation starts with the first pulse and the ablation depth increases linearly with the number of pulses. In this case, incubation is not significant, and we assume that absorption processes are only related to pyrene.

The effective absorption coefficient α_{eff} is very different from the linear absorption coefficient α_0. The latter depends only on the material and makes reference to the way in which it absorbs the photons. The effective absorption coefficient α_{eff} relates to how the material is ablated by the laser pulse, however. It is not to be seen as an inherent material constant but rather depends on a combination of the characteristic parameters of the material and of the laser pulse. More specifically, it depends on the local linear absorption coefficient (relates to how the material locally absorbs the photons and converts the optical energy into thermal energy), the local thermal diffusion length and the absorption of the incoming laser pulse by the ablation-created plasma, which reduces the energy really absorbed by the target. These parameters change dynamically during the laser ablation. Therefore, the effective absorption coefficient is difficult to interpret even if relatively simple to measure, since it relates to the equilibrium between heating (linear absorption) and cooling by heat conduction (thermal diffusion length). Nevertheless, it can be used for a macroscopic description of the ablation.

To assess the impact of pyrene functionalization on α_{eff} and F_{th}, for each kind of sample a matrix of cavities was etched in which two parameters were varied: the fluence (from 0.03 to ~1.7 J/cm^2) and the number of pulses (1, 2, 5, 10, and 15 pulses). The depth of each cavity was measured and plotted against the number of pulses on graphs similar to that of Figure 5. Even though ablation starts with the first pulse, depth measurements of several multiple-pulse cavities increase the precision of the measured ablation depth per pulse (for almost all linear regressions, R^2 > 0.99). The ablation depths per pulse obtained from these graphs are plotted against the fluence (in log scale) for all samples in Figure 6.

The ablation threshold fluence F_{th} is a delicate parameter to extract since for fluences just before the ablation threshold there is a slight volume expansion, making it difficult to determine exactly at which fluence ablation starts. Equation 1 was used to fit the data linearly on the semi-log plots of Figure 6 to extract α_{eff} ; F_{th}. α_{eff} corresponds to the inverse of the slope of the fit, and F_{th} corresponds to the value of the fit when the ablation depth goes to zero. Only the data for the lowest fluences were used to extract F_{th}. The corresponding values along with relative errors are reported in Table 4. In the fluence range we are studying, eq 1 describes well the ablation depth per pulse, which is mostly linear with the logarithm of the fluence. The only deviation is a saturation at high fluence for PMMA doped with 2% of the alkylpyrene derivative (Figure 6b). Because this phenomenon is specific to this sample and unexplained, we did not include these data to compute α_{eff}. For the grafted samples, α_{eff} changes at higher fluences. We report the values according to the range in Table 4 and discuss them hereafter.

Increasing the doping concentration of pyrene in PMMA impacts both parameters: the threshold fluence decreases and the effective absorption coefficient (the inverse of the slope) increases. For higher density of absorbing species, the laser energy penetrates less into the material and is deposited in a smaller volume. Consequently, the ablation starts at a smaller fluence but the cavities obtained at higher fluences are shallower (higher effective absorption coefficient). The trend is the same regardless of the material.

The effective absorption coefficients and threshold fluences of pyrene and alkypyrene derivative samples are similar within experimental error. The increase of the linear absorption coefficient α_0 of an alkylpyrene derivative sample compared with that of a pyrene sample at the same dopant concentration (see Figure 3) does not seem to change the ablation, either because the change is too small to see or because other parameters are modified. Therefore, merely functionalizing the dopant does not impact laser ablation of doped-PMMA.

The pyrene-grafted PMMA samples, on the other hand, clearly display a different behavior from that of the doped PMMA samples. The threshold fluences for 1 and 4% of pyrene are significantly lower than for both doped samples (Table 4).

dx.doi.org/10.1021/am404376e | ACS Appl. Mater. Interfaces 2014, 6, 41−48

Even for the 2% pyrene samples, the difference between the alkylpyrene derivative and the grafted samples is large enough to be significant since it has to be remembered that the real molar concentrations are different (1.94% for pyrene-doped samples and 1.59% for pyrene-grafted samples). A big difference between the alkylpyrene derivative and the grafted pyrene is that for the latter compound there is a covalent bond linking the chromophore to the side-chain of the polymer matrix. This bond is likely to change the way in which the energy absorbed by the pyrene molecules is transmitted to the polymer chains. In other words, there may be a difference in the thermal as well as the optical properties of pyrene-grafted PMMA. It can be expected that the thermal and vibronic energy transfer is more efficient when pyrene molecules are grafted. This may explain the lower threshold fluence of grafted samples compared with that of the doped samples. The lowering of the threshold fluence allows clean cavities to be etched at lower fluence.

We sometimes observed inhomogeneities in cavities etched at low fluence for doped samples (Table 3). This suggests that just spreading pyrene or the alkylpyrene derivative inside PMMA does not guarantee a homogeneous dispersion. When the fluence is too close to the ablation threshold, some areas of the cavity do not receive enough energy to be ablated away, partly because the pyrene concentration fluctuates. On the other hand, cavities etched in pyrene-grafted PMMA always displayed regular profiles even at fluences close to the threshold. This may be partly explained by the covalent bonding of the chromophores on the polymer chains, which forces the dispersion.

In Figure 6c, we notice that for PMMA grafted with pyrene the slope of the curve changes slightly above 0.6 J/cm^2. The corresponding effective absorption coefficients are reported in Table 4. Changes in α_{eff} might indicate a change in the etching mechanisms.[2] Ablation rates and effective absorption coefficients are also very much alike for the higher fluence range. Other polymers behave in the same way at high fluences and this has been attributed to a screening effect from desorbed ablation products.[23] Since α_{eff} changes notably only for the grafted polymer, we can postulate that the better thermal transfer previously mentioned plays a role. It could induce a higher temperature in the material and produce an ablation plasma with higher electrical density and temperature, which would increase the shielding of the laser pulse.

CONCLUSIONS

The KrF laser ablation of PMMA modified with pyrene-based chromophores has been investigated. The effect of doping PMMA films with pure pyrene has been discussed in the literature. To improve the dispersion homogeneity and the material ablation response, we introduced functionalization of the pyrene molecule by doping PMMA with an alkylpyrene derivative and grafting the pyrene molecule on the side chains of PMMA. Fluorescence spectroscopy showed that functionalization of pyrene did not suppress pyrene aggregation, which appeared in the three kinds of samples above a concentration of 2% of pyrene. The way in which pyrene is dispersed into the polymer does not change the quality of ablation (smoothness of bottoms and edges of cavities, projections and redepositions). Quantitative measurements of the ablation depth for the three materials revealed that when the chromophore concentration increases α_{eff} increases and F_{th} decreases. Doping with a substituted pyrene does not change the ablation parameters significantly. When the chromophore is grafted to the PMMA chains, ablation rates become similar for fluences above 0.6 J/cm^2 regardless of the pyrene proportion, and threshold fluences decrease significantly. Because this does not occur when the PMMA is doped with an alkylpyrene derivative, it may result from other mechanisms than the increased linear absorption coefficient because of pyrene functionalization. These may include modification of the heat transmission from excited pyrene molecules to PMMA chains and better large-scale homogeneity, thanks to the covalent bonding of the pyrene on the polymer.

ASSOCIATED CONTENT

Supporting Information

SEC UV and refractive index overlaid signals for pure PMMA and 4% pyrene-grafted PMMA, and NMR spectra for the pyrene-grafted MMA monomers and the pyrene-grafted PMMA copolymer. This material is available free of charge via the Internet at http://pubs.acs.org.

AUTHOR INFORMATION

Corresponding Author

*E-mail: biver@lp3.univ-mrs.fr.

Notes

The authors declare no competing financial interest.

ACKNOWLEDGMENTS

This work has been done in the frame of the CIMPACA project. The authors express their appreciation to Dr. Thomas Lippert for helpful discussions, to Spectropole of Aix-Marseille University for the use of their nuclear magnetic resonance spectrometer, and to the CP2M Platform of Aix-Marseille University for the use of their confocal microscope. This work has been supported by the French General (CG13) and Regional (CRPACA) Councils, FEDER, Institut Carnot STAR and ARCSIS.

REFERENCES

(1) Mathews, S. A.; Charipar, N. A.; Metkus, K.; Piqué, A. *Photonics Spectra* **2007**, *41*, 70−74.
(2) Lippert, T.; Hauer, M.; Phipps, C. R.; Wokaun, A. *Appl. Phys.* **2003**, *77*, 259−264.
(3) Lazare, S.; Granier, V. *Laser Chem.* **1989**, *10*, 25−40.
(4) Dyer, P. E. *Appl. Phys.* **2003**, *77*, 167−173.
(5) Allen, N. S., Ed. *Photochemistry and Photophysics of Polymer Materials*; Wiley: Hoboken, NJ, 2010.
(6) Nagel, M.; Hany, R.; Lippert, T.; Molberg, M.; Nüesch, F. A.; Rentsch, D. *Macromol. Chem. Phys.* **2007**, *208*, 277−286.
(7) Fukumura, H.; Takahashi, E.; Masuhara, H. *J. Phys. Chem.* **1995**, *99*, 750−757.
(8) Wang, J.; Niino, H.; Yabe, A. *Jpn. J. Appl. Phys.* **1999**, *38*, L761 LP−L763.
(9) Lippert, T.; Dickinson, J. T. *Chem. Rev.* **2003**, *103*, 453−86.
(10) Chuang, T. J.; Hiraoka, H.; Mödl, A. *Appl. Phys. A: Solids Surf.* **1988**, *45*, 277−288.
(11) Masuhara, H.; Hiraoka, H.; Domen, K. *Macromolecules* **1987**, *20*, 450−452.
(12) Blanchet, G. B.; Cotts, P.; Fincher, C. R. *J. Appl. Phys.* **2000**, *88*, 2975−2978.
(13) Fujiwara, H.; Hayashi, T.; Fukumura, H.; Masuhara, H. *Appl. Phys. Lett.* **1994**, *64*, 2451−2453.
(14) Winnik, F. M. *Chem. Rev.* **1993**, *93*, 587−614.
(15) Búcsiová, L.; Hrdlovic, P.; Chmela, S. *J. Photochem. Photobiol. Chem.* **2001**, *143*, 59−68.

(16) Palmans, J. P.; Swinnen, A. M.; Desie, G.; Van Der Auweraer, M.; Vandendriessche, J.; De Schryver, F. C. *J. Photochem.* **1985**, *28*, 419−431.
(17) Jiang, J.; Tong, X.; Zhao, Y. *J. Am. Chem. Soc.* **2005**, *127*, 8290−8291.
(18) Mann, K. R.; Ohlenbusch, J.; Westphal, V. In *Proceedings of SPIE: Third International Workshop on Laser Beam and Optics Characterization*; Morin, M., Giesen, A., Eds.; Quebec City, Canada, July 8, 1996 ; SPIE: Bellingham, WA, 1996; Vol. *2870*, pp 367−377.
(19) Marsh, N. D.; Mikolajczak, C. J.; Wornat, M. J. *Spectrochim. Acta, Part A* **2000**, *56*, 1499−1511.
(20) Niko, Y.; Kawauchi, S.; Otsu, S.; Tokumaru, K.; Konishi, G. *J. Org. Chem.* **2013**, *78*, 3196−3207.
(21) Itaya, A.; Kurahashi, A.; Masuhara, H.; Taniguchi, Y.; Kiguchi, M. *J. Appl. Phys.* **1990**, *67*, 2240−2244.
(22) Nijegorodov, N.; Vasilenko, V.; Monowe, P.; Masale, M. *Spectrochim. Acta, Part A* **2009**, *74*, 188−194.
(23) Lippert, T. UV Laser Ablation of Polymers: From Structuring to Thin Film Deposition. In *Laser-Surface Interactions for New Materials Production*; Miotello, A., Ossi, P. M., Eds.; Springer: Berlin, 2010; Vol. *130*, pp 141−175.